

# Quantum charge pumping and electric polarization in Anderson insulators

Chyh-Hong Chern\*

*Institute for Solid State Physics, University of Tokyo, Kashiwanoha, 5-1-5, Kashiwa 277-8581, Japan*

Shigeki Onoda and Shuichi Murakami

*CREST, Department of Applied Physics, University of Tokyo, 7-3-1, Hongo, Tokyo 113-8656, Japan*

Naoto Nagaosa

*CREST, Department of Applied Physics, University of Tokyo, 7-3-1,*

*Hongo, Tokyo 113-8656, Japan, and Correlated Electron Research Center,*

*National Institute of Advanced Industrial Science and Technology, 1-1-1, Higashi, Tsukuba, Ibaraki 305-8562*

(Dated: July 13, 2018)

We investigate adiabatic charge pumping in disordered system in one dimension with open and closed boundary conditions. In contrast to the Thouless charge pumping, the system has no gap even though all the states are localized, i.e., strong localization. Charge pumping can be achieved by making a loop adiabatically in the two-dimensional parameter space of the Hamiltonian. It is because there are many  $\delta$ -function-like fluxes distributed over the parameter space with random strength, in sharp contrast to the single  $\delta$ -function in the pure case. This provides a new and more efficient way of charge pumping and polarization.

## INTRODUCTION

The quantum dynamics of the charge in insulators is a rich and non-trivial issue even in the d.c. limit. Of course, the d.c. conductivity vanishes, but this does not mean that charge motion is frozen in the insulators. One example is the ferroelectricity and electric polarization in insulators. The classical definition of the electric polarization  $\vec{P} = \int d\vec{r} \vec{r} \rho(\vec{r})$  ( $\rho(\vec{r})$ : charge density) fails for the extended Bloch wave functions since the  $\vec{r}$  is unbounded. This difficulty is avoided by considering instead the new definition for the *difference* of the polarization [1, 2, 3, 4, 5],

$$\Delta \vec{P} = \int_0^T d\tau \frac{d\vec{P}}{d\tau}, \quad (1)$$

where the change of the polarization between the initial and final states are given by the integral of the polarization *current* during the adiabatic change of the parameters  $\vec{Q} = (Q_1, Q_2, \dots, Q_n)$  such as the atomic displacements. One can usually choose the initial state with the inversion symmetry without electric polarization, and (1) uniquely determines the polarization of the final state of our interest. Here by using  $\frac{d\vec{P}}{d\tau} = \frac{d\vec{P}}{dQ_i} \frac{dQ_i}{d\tau}$ , the  $\mu$ -component of  $\Delta \vec{P}$  is expressed as

$$\Delta P_\mu = \int_C d\vec{Q} \cdot \frac{dP_\mu}{d\vec{Q}} \quad (2)$$

with the path  $C$  specified by  $\vec{Q} = \vec{Q}(\tau)$ . What is found by Resta [3] and King-Smith and Vanderbilt [4] is that  $\frac{dP_\mu}{d\vec{Q}}$  can be represented by the Berry phase, which fits to the first-principle band calculation. Then the question arises, “Is there any path ( $C$ ) dependence of the polarization?”. It is clear that there is no parametrization

dependence since we consider the adiabatic change, but the different path  $C_1$  and  $C_2$  in the  $\vec{Q}$ -space might lead to the different values of  $\Delta \vec{P}$ . This is related to the single-valueness and Chern number of the Bloch wavefunction. Onoda *et al.* addressed this problem as follows by analyzing the one-dimensional two-band models characterized by the three dimensional  $\vec{Q}$  [6, 7]. There appears a singular line, i.e., string, in the  $\vec{Q}$ -space corresponding to the trajectory of the monopole (band crossing point) as the momentum  $k$  moves, which acts as the “current circuit” to produce the “magnetic field”  $\frac{d\vec{P}}{d\vec{Q}}$  via the Biot-Savart law. Away from the string, the system is always gapped, and insulating. When the adiabatic change of the parameter  $\vec{Q}$  makes a loop enclosing the string, the charge is pumped during this process, which is quantized to be an integer multiple of  $e$  since the strength of the “current” is quantized. This is a realization of the quantum charge pumping first proposed by Thouless [8]. This analogy to the magnetostatics says that the polarization is path independent as long as the loop  $C = C_1 + (-C_2)$  does not enclose the string. This is usually the case because the change of the parameter  $\vec{Q}$  is rather small and we need the huge variation of  $\vec{Q}$  to enclose the string, i.e., gapless states. In other words, the ferroelectricity can be regarded as “a fraction of the quantum charge pumping”.

This charge pumping can be regarded as the rigid shift of the wavefunction due to the change in the external parameters such as the atomic positions. It is natural when the wavefunction consists of the Bloch states extended over the whole sample, and then the quantum interference pattern is modified by the external parameters. One can estimate roughly how much the charge is pumped as below. Let the dimension of the parameters be the energy. Then the distance between the physically realized set of parameters and that of gapless states, i.e.,

string, is the energy gap  $E_G$ . When  $\Delta$  be the change of the parameters in unit of energy, the angle subtended by this *segment* in parameter space is roughly estimated as  $2\pi\Delta/E_G$ . Since the  $2\pi$  winding corresponds to unit charge  $e$  shift by one lattice constant  $a$ , i.e.,  $P_0 = ea$ , the polarization is roughly given by  $P = ea\Delta/E_G$  [6]. Therefore one can enhance the dielectric response by reducing  $E_G$ , or enlarging  $\Delta$ . One possible method to reduce  $E_G$  is by introducing disorder, by which even the gapless insulator can be realized. However, the electron wavefunctions are no longer the extended Bloch states in the presence of the disorder, and one needs to worry about the localization, i.e., Anderson localization. When all the states are strongly localized, one can not transmit the phase information through the sample, and hence can not expect the charge pumping either. On the other hand, as can be seen from the above explanation, the charge pumping is closely related to the topological nature of the wavefunctions in the parameter space, which is robust against the disorder to some degree. For example, in the two dimensional electron systems under strong magnetic field, there occur discrete extended states *protected by the topology*. Namely, the Chern number is carried by the extended states only, which is not destroyed by the weak disorder. Therefore similar problem arises even for the one-dimensional systems which we study below. Niu and Thouless [9] was the first to study the stability of the charge pumping against the weak disorder by a topological argument. Even though all the states are localized, the charge pumping was shown to be unchanged as long as the gap remains finite. However, questions still remain such as what is the physical mechanism of the charge pumping through the localized states and what happens when the gap collapses.

In this paper, we study the effect of the disorder on the charge pumping and dielectric response in a one-dimensional model for insulators. Combining the numerical simulations and analytic considerations, we reveal the physical picture of the charge pumping by the localized states both in the case of open boundary condition and periodic/twisted boundary condition. The former one is more relevant to the experimental situation such as the FeRAM (ferroelectric random access memory) where the leads are attached to the thin film of insulators, while the latter is more appropriate to see the role of topology. We have published a Letter focusing on the open boundary condition [10]. This paper provides the full details of the formulation, calculations, and additional results on the open system, as well as new results on the periodic/twisted boundary condition.

The plan of this paper follows. In section II, a model for disordered insulator showing the charge pumping is introduced. Its analysis with the open boundary condition is given in section III, including the detailed description of the resonant tunnelling mechanism. In section IV given the analysis of the model in the three dimensional

parameter space including the angle  $\alpha$  for the twisted boundary condition, and the role of magnetic monopoles in this space. Section V is devoted to the conclusions.

## A MODEL FOR DISORDERED INSULATOR

The minimal model for ferroelectrics is given by the following ionic dimer model;

$$H_{\text{pure}} = -\frac{1}{2} \sum_{i=1}^L (t_{\text{n.n.}} - (-)^i Q_2) (c_{i+1}^\dagger c_i + h.c.) + \sum_{i=1}^L (-)^i Q_1 c_i^\dagger c_i. \quad (3)$$

Here,  $c_i$  and  $c_i^\dagger$  are the annihilation and creation operators of the electron at the site  $i = 1, \dots, L$  with  $L$  being the number of sites in the system. For open system attached to leads at the both ends,  $c_{L+1}$  and  $c_{L+1}^\dagger$  represents those operators in one of the leads, while for closed system, they are understood as  $c_1$  and  $c_1^\dagger$ .  $t_{\text{n.n.}}$  is the transfer integral.  $Q_1$  and  $Q_2$  represent the alternations of the local ionic level and the bond dimerization, respectively. The spin degree of freedom is omitted for simplicity. Then, of our interest is the half-filling case relevant to the ferroelectrics. Although this model might look special, it represents the two essential features of the ferroelectrics, i.e., (i) the two species of the ions characterized by the level alternation  $Q_1$  and (ii) relative shift of the atomic positions described by the dimerization  $Q_2$ . It corresponds to the ferroelectricity in e.g. BaTiO<sub>3</sub>, where Ti and O are dimerized to produce the polarization [11]. It can be also applied to the quasi-one dimensional ferroelectric materials such as organic charge transfer compounds TTF-CA [12] and (TMTTF)<sub>2</sub>X [13].

The Hamiltonian  $H_{\text{pure}}$  under the periodic boundary condition yields two bands[6]

$$\varepsilon_{\pm}(k) = \pm \sqrt{t_{\text{n.n.}}^2 \cos^2 k + Q_1^2 + Q_2^2 \sin^2 k}. \quad (4)$$

Experimentally, the parameters  $\vec{Q} \equiv (Q_1, Q_2)$  can be controlled by applying the electric field  $E$  along the polarization direction and the pressure  $p$  as follows. Electrons at high and low density sites shift in relatively opposite directions, as shown in open arrows of Fig. 1 (b), changing the dimerization  $Q_2$  by  $\delta Q_2 \propto eEQ_1$ . Simultaneously, within each dimer, a level difference  $Q_1$  changes by  $\delta Q_1 \propto -eEQ_2$  as illustrated by black arrows in Fig. 1 (b). Therefore, the electric field  $E$  mainly controls the angle

$$\theta = \arctan(Q_2/Q_1). \quad (5)$$

Applying the pressure, one can increase the hybridization, and then reduces the ratio  $Q/t_{\text{n.n.}}$  with

$$Q = \sqrt{Q_1^2 + Q_2^2}. \quad (6)$$

To discuss the quantum relaxor behavior, we introduce the on-site random potential  $v_i$  to the Hamiltonian given by (3);

$$H = H_{\text{pure}} + \sum_{i=1}^L v_i c_i^\dagger c_i. \quad (7)$$

The type of the random distribution takes either a uniform distribution or an alloy model, which are shown in Fig. 2. In the following, we study effects of on-site disorder on dielectric properties in both open and closed systems, particularly focusing on the topological aspects.

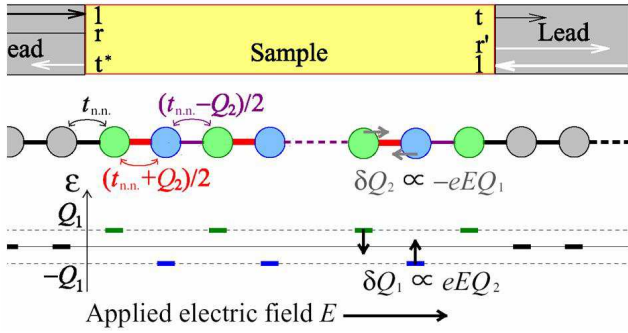


FIG. 1: (Color online) Ionic dimer system sandwiched by the leads.

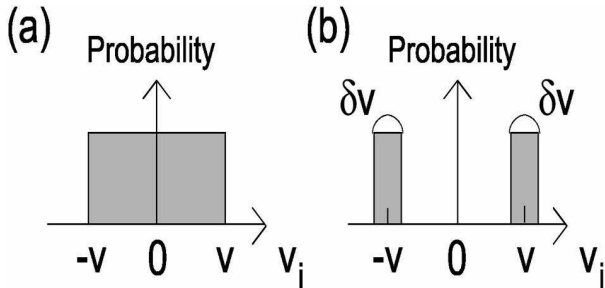


FIG. 2: (a) Uniform distribution of the on-site random potential. (b) Alloy model for the on-site random potential, which mimics effects of substitution in alloys.

## OPEN BOUNDARY CONDITION

In this section, dielectric property of disordered insulators connected to the leads is studied theoretically. This corresponds to the realistic situation in FeRAM devices, where the polarization is measured by the integrated current flowing in the leads. Especially in nano-scale samples of the FeRAM, the quantum nature of the polarization is expected to play essential roles via novel quantum interference as discussed in the introduction [6, 8]. Namely, a theory for the nano-scale capacitance is called for where the quantum coherence is attained all through the sample. From the viewpoint of the applications, it is required to achieve (i) a magnitude of the polarization larger than  $10 \mu\text{C}/\text{cm}^2$ , (ii) a smaller leak current than  $0.1\text{--}1 \mu\text{A}/\text{cm}^2$ , and (iii) a dielectric constant larger than 300 [14]. By introducing disorder, one can also suppress the dissipation by leak current due to the strong localization effect [9, 15] in addition to the reduction of the gap and enhanced dielectric response. In fact, a similar disorder-driven enhanced response has been found in relaxor ferroelectrics [16, 17, 18] and pinned charge density waves [19], although its mechanism is due to a classical mesoscopic cluster formation analogous to spin glass systems.

In the disordered case with all the states being localized, the charge transfer occurs through the resonant tunnelling. The quantum nature is topologically protected. Crossover from the quantized charge pumping in bulk insulator [8] to that of quantum dot [20] is clarified in the control parameter plane as a function of sample size and disorder strength [21, 22, 23]. Then, we theoretically propose the enhancement of the dielectric response of insulators by disorder in nanoscopic/mesoscopic multichannel systems, with the required time for the dissipationless adiabatic charge displacement being estimated. Application of this phenomenon to memory devices, like ferroelectric random access memory (FeRAM) [14], is also discussed.

### Single-channel problem for uniformly distributed random potential

We consider an insulating electronic system sandwiched by leads (electrodes) as shown in Fig. 2(a). For simplicity, we take a one-dimensional (single-channel) model, but the extension to higher dimensional (multi-channel) cases is straightforward as discussed later.

We take the total Hamiltonian

$$H_{\text{tot}} = H + H_{\text{lead}} \quad (8)$$

with  $H$  and  $H_{\text{lead}}$  being given by (7) and

$$H_{\text{lead}} = -\frac{t_{\text{n.n.}}}{2} \left( \sum_{i=0}^{-\infty} + \sum_{i=L}^{\infty} \right) (c_{i+1}^\dagger c_i + h.c.), \quad (9)$$

respectively. This model is schematically shown in Fig. 1 (b). The Green's function  $G_{i,i'}(\varepsilon)$  for the above model is readily obtained from the recursion formula in the form of the continued fraction [24]. Here, we can concentrate on the case where the chemical potential is located at the zero energy.

We adopt the Landauer-Büttiker formalism [24, 25], where the sample is regarded as a *scatterer* characterized by the scattering  $S$ -matrix

$$S = \begin{pmatrix} r & t \\ t^* & r' \end{pmatrix}. \quad (10)$$

Here, the reflection coefficients  $r$  and  $r'$ , and the transmission coefficient  $t$  (see Fig. 1) can be calculated from the Green's functions [24]. The transmittance through the sample and the reflectance at the both ends are expressed as

$$T = |t|^2, \quad (11)$$

$$R = |r|^2 = |r'|^2 = 1 - T, \quad (12)$$

respectively. Then, we employ the Brouwer's formula [26, 27], which has been successfully applied to the charge pumping in metallic quantum dot systems [20]: the charge  $\Delta q$  pumped from the left to the right during an adiabatic change of parameters  $\vec{Q}$  along a path  $C$  is given by [26]

$$\Delta q = e \int_C \frac{d\vec{Q}}{2\pi} \cdot \text{Im} \left( r^* \vec{\nabla}_Q r + t \vec{\nabla}_Q t^* \right). \quad (13)$$

Therefore, even in the perfectly reflecting case  $t = 0$ ,  $|r| = 1$ , charge can be pumped by controlling the phase  $\varphi$  of  $r = e^{i\varphi}$  [28].

Let us start with the pure case ( $v_i = 0$ ). Without the random potential  $v_i$ , the bulk system has an energy gap

$$E_{G0} = 2\sqrt{Q_1^2 + \text{Min}\{t_{n,n.}^2, Q_2^2\}}. \quad (14)$$

This gap closes at  $\vec{Q} = \vec{0}$ , where the metallic conduction occurs. This yields a vortex center of the reflective coefficients  $r$  and  $r'$ . By means of the continued-fraction expansion of the Green's function, an analytic form of  $r$  in the thermodynamic limit  $L \rightarrow \infty$  is obtained as

$$r = -\frac{Q_1^2 + t_{n,n.}Q_2 + Q\sqrt{t_{n,n.}^2 + Q_1^2} + 2it_{n,n.}Q_1}{Q_1^2 + t_{n,n.}Q_2 + Q\sqrt{t_{n,n.}^2 + Q_1^2} - 2it_{n,n.}Q_1} \quad (15)$$

where  $Q \equiv \sqrt{Q_1^2 + Q_2^2}$ . The panels (a1) and (b1) of Fig. 3 show the reflectivity  $R = |r|^2$  for  $L = 10001$  and the phase  $\varphi$  of  $r$  for  $L \rightarrow \infty$  without randomness. Here the phase winds by  $2\pi$  around  $\vec{Q} = (0, 0)$ , forming a “vortex” at which  $r = 0$  and  $|t| = 1$ . In the thermodynamic limit  $L \rightarrow \infty$ ,  $R = 1$  and  $T = 0$  hold except at the vortex center. For finite-size systems, the transmittance  $T$  behaves as  $e^{-L/\xi_0}$  with  $\xi_0 = t_{n,n.}/E_{G0}$ . Therefore the size

of the region in the  $\vec{Q}$  space with a large  $T$  is of the order of  $t_{n,n.}/L$  for a large  $L$ . Namely the vortex corresponds to the gapless case, where the extended state at the Fermi energy carries the charge and causes the perfect transmittance. Remarkably, this perfect-transmission point  $\vec{Q} = \vec{0}$  governs topological properties of the system in the whole  $\vec{Q}$  plane in a non-local way. When we adiabatically change the parameter  $\vec{Q}$  along a cycle around  $\vec{Q} = \vec{0}$  at which the transmittance  $T$  vanishes, the charge  $e$  is pumped and the polarization changes by  $\pm 2ea$  ( $a$ : lattice constant) according to the Brouwer's formula (13). The vortex is almost isotropic at least in the vicinity of its core. Then, a pumped charge due to a small change  $\vec{\Delta}$  of  $\vec{Q}$  is expressed as  $q \sim (\phi/2\pi)e \sim (|\vec{\Delta}|/E_G)e$ , where  $\phi$  represents a change in the polar angle of the vector  $\vec{Q}$ . Therefore one can enhance the pumped/displaced charge by enlarging the angle  $\phi$  subtended by  $\vec{\Delta}$  around the gapless point. This quantized charge pumping [8] through the adiabatic cyclic change of  $\vec{Q}$  is consistent with the results previously found in the periodic system [6] by using the Berry-curvature formulation of the electric polarization [1].

Now we turn on the disorder in order to reduce the gap  $E_G$ . In the  $\vec{Q}$  plane, the region of  $|\vec{Q}| \lesssim v$  becomes gapless, while the Anderson localization seriously affects the transport properties [15, 29]. In one dimension, the effect is pronounced and all the states are localized [30, 31, 32]. On the other hand, the total vorticity  $N_v$  is an integer topological number, and is robust under a continuous change of parameters including the disorder strength. Therefore, even with disorder,  $N_v$  remains unity. Namely, there should exist at least one vortex ( $r = 0$ ) in the  $\vec{Q}$  plane; thus perfect transmittance  $|t| = 1$  occurs even though all the states are strongly localized. This is a remarkable consequence from the quantum and topological property of the system, and is in sharp contrast to usual classical tunnelling through disordered insulators.

In Figs. 3 (a2) and (b2), we show our numerical results of  $R$  and  $\varphi$  for  $L = 101$  with a uniform random distribution  $v_i \in [-v, v]$  for the disorder strength  $v = 0.25t_{n,n.}$ . The vortex center of the perfect transmittance  $T = 1$  and  $R = 0$  shifts in the  $\vec{Q}$  space. Besides, an anisotropy develops in the shape of the region of relatively high transmittance  $T$ . We further calculate  $R$  and  $\varphi$  for larger systems, which are shown in (a3) and (b3) for  $L = 201$  and in (a4) and (b4) for  $L = 401$ . There, it is evident that the vortex core, which is almost isotropic without the disorder, rapidly evolves into the highly anisotropic one. This is associated with an increase of the ratio  $L/\xi$  by increasing the system size. Figure 4 shows the local density of states  $D_i$  of site  $i (= 1, \dots, L)$ , which has been calculated when  $\vec{Q}$  is located at the vortex center  $\vec{Q}_c$  corresponding to each case of  $L = 101, 201$  and  $401$  for  $v/t = 0.25$ . When  $L$  is equal to 101 or smaller, the state at this energy is

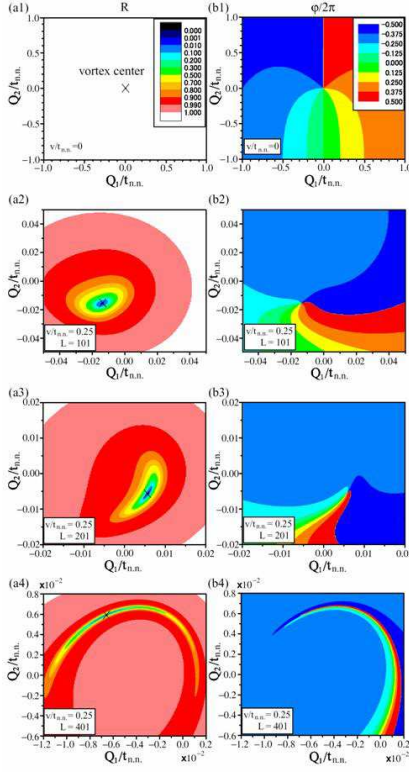


FIG. 3: (Color) Reflectance  $R = |r|^2$ , and the phase  $\varphi = \arg r$ . (a1), (b1): clean bulk system. (a2), (b2): disordered system of finite size  $L = 401$  with the random potential of the strength  $v/t_{n,n} = 0.5$ . The color code given in (a1)/(b1) also applies to (a2,3)/(b2,3). In the white region in (a1,2,3),  $R$  is the unity within the accuracy of  $10^{-4}$ .

extended over the sample. However, with increasing  $L$ , the state is almost localized in the middle of the sample. The spatial extension of the wave function, i.e., the localization length  $\xi$ , can be explicitly evaluated from the second moment of  $D_i$  as the inverse participation ratio;

$$\xi_{IPR} = (\sum_i D_i)^2 / \sum_i D_i^2. \quad (16)$$

We obtain  $\xi_{IPR} = 51.4, 80.8, 76.4$  and  $84.7$  for  $L = 101, 201, 401$  and  $501$ , respectively around the vortex center, indicating that  $\xi_{IPR}$  almost saturates about 80 sites for  $v/t = 0.25$ .

In this anisotropic “wing”,  $\varphi$  changes rapidly. The width  $Q_W$  of the anisotropic wing decays exponentially as  $\exp(-L/\xi)$  with increasing  $L$ , as shown in Fig. 5.

In the rest of this subsection, we comment on the relation of the charge displacement discussed above to the charge pumping through a *metallic dot* [20] weakly connected with two leads. In the metallic dot systems, a charge is pumped from one lead to the other by changing the heights of potential barriers between the dot and

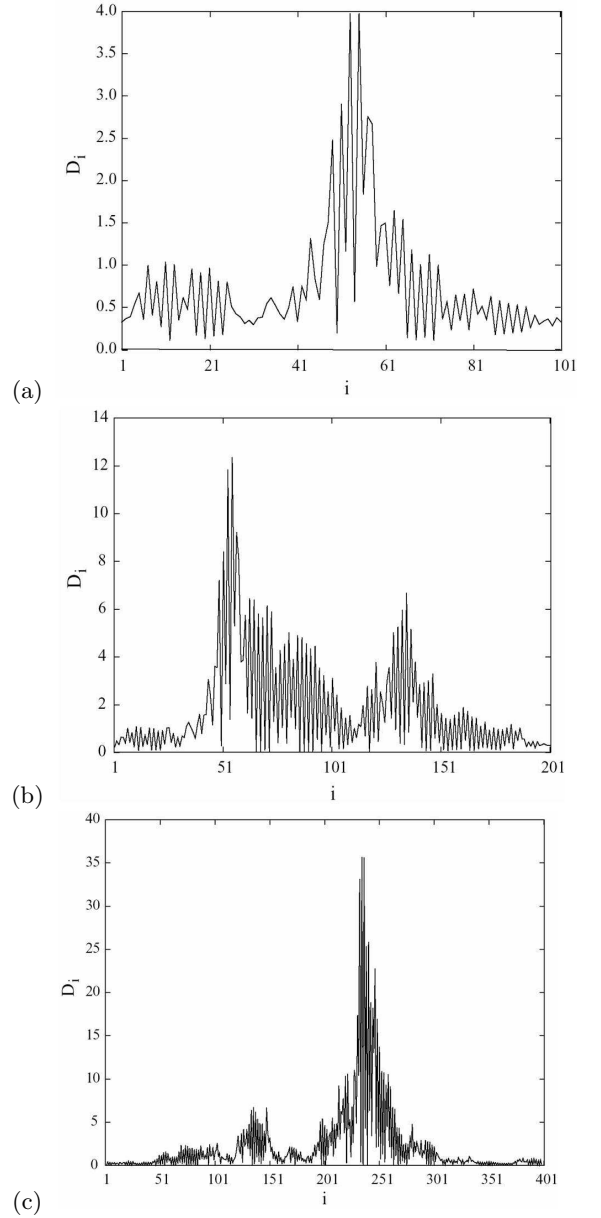


FIG. 4: Local probability  $D_i$  of the state at the vortex for (a)  $L = 101$ , (b)  $L = 201$ , and (c)  $L = 401$  in the presence of uniformly distributed random potential  $v_i \in [-v, v]$  with  $v = 0.25t_{n,n}$ .

the neighboring leads [26]. Since the system is metallic, the pumped charge is not quantized in this case. Here, the main source of the pumping is a finite transmittance but not the phase of reflection coefficient. With increasing the system size, it crosses over to the opposite regime with vanishing transmittance studied in this paper. In the present theory, the charge pumping comes from the vortex of the reflection coefficient. Therefore, it is topologically protected against disorder. This topological constraint guarantees the applicability of the resonance tunnelling [33], only near the vortex.

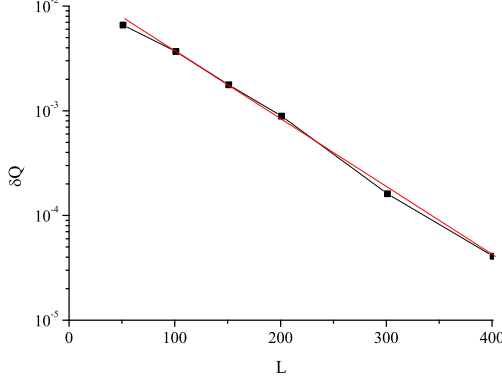


FIG. 5: The minimum width  $\delta Q$  for  $R$  determined at  $R = 0.3$  as a function of  $L$ .

### Resonance tunnelling

In order to understand transport properties of such one-dimensional disordered systems, it is sometimes useful to consider an effective model with the potential having high double peaks. In this model, well-defined localized eigenstates exist between the two potential peaks, and any transport between two ends of the system occurs via the localized states through tunnelling. While such tunnelling has exponentially small probability, it occurs when the Fermi energy of the leads is equal to one of the eigenenergies of the localized states, namely when the resonance takes place. This picture of transport in disordered systems is called “resonance tunnelling” [33].

Here we describe the resonance-tunnelling theory, following Ref. 33, and will see whether it fits with the present model with disorder. We define an effective model of “resonance tunnelling” as described by the Schrödinger equation  $\Psi''(x) + (k^2 - V(x))\Psi(x) = 0$  where  $\hbar^2 k^2 / 2m$  is the particle energy, and the effective potential  $V(x)$  has two peaks as shown in Fig. 6. It is not trivial whether the numerical results of our model (3) fits well with this resonance-tunnelling picture. The present model has many valley and peaks, due to on-site randomness, and is not similar with Fig. 6. Nevertheless, when the localization length  $\xi$  is much shorter than the system size, it is indeed the case as we see by fitting our numerical results well by the picture of resonance tunnelling. The basic reason for the applicability of resonance tunnelling is that the topology guarantees an existence of a perfect-transmittance point, i.e., the resonant tunnelling in the two-dimensional parameter space  $(Q_1, Q_2)$ , in spite of the complexity of the potential shape in the model.

First let us consider an open system attached to two ideal leads which are connected to reservoirs. The Fermi energy  $E_F$  is tuned at one’s disposal, and we assume that

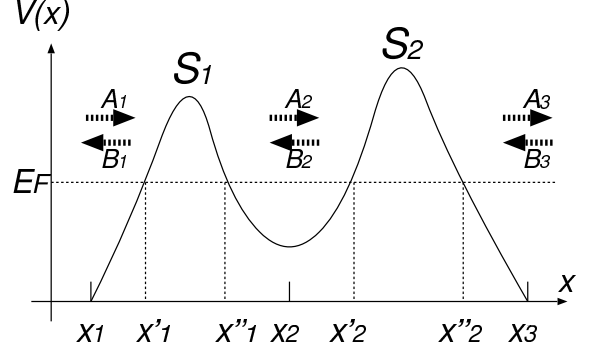


FIG. 6: Potential profile for the effective model of resonance tunnelling. Heights of the two potential peaks are characterized by  $S_1$  and  $S_2$ .

the potential peaks are much higher than  $E_F$ . An effective wave number  $k(x) \equiv \sqrt{k^2 - V(x)}$  becomes imaginary inside the potential peaks, and the particle tunnels through the peaks. One of the eigenstates at the left lead ( $x < x_1$ ) is given by  $\Psi_1(x) \sim \exp(ik_1(x - x_1))$ , where  $k_1 = k(x_1)$ . The time-reversal symmetry of the system requires that the complex conjugate  $\Psi_1^*(x)$  is also an eigenstate. At the potential valley around  $x = x_2$  we can also consider eigenstates with  $\Psi_2(x) \sim \exp(ik_2(x - x_2))$  and  $\Psi_2^*(x)$ , where  $k_2 = k(x_2)$ . Thus general eigenstates around  $x = x_1$  and around  $x = x_2$  are given as  $\Psi(x) = A_1\Psi_1(x) + B_1\Psi_1^*(x)$  and  $\Psi(x) = A_2\Psi_2(x) + B_2\Psi_2^*(x)$ , respectively. Next we introduce the transfer matrix  $\Theta_1$  from  $x_2$  to  $x_1$

$$\begin{pmatrix} A_1 \\ B_1 \end{pmatrix} = \Theta_1 \begin{pmatrix} A_2 \\ B_2 \end{pmatrix}, \quad (17)$$

where  $\Theta_1$  is a  $2 \times 2$  matrix. Time-reversal symmetry requires the transfer matrix  $\Theta$  to be of the form

$$\Theta_1 = \left(\frac{k_2}{k_1}\right)^{\frac{1}{2}} \begin{pmatrix} \cosh(S_1)e^{i\alpha_1} & \sinh(S_1)e^{i\beta_1} \\ \sinh(S_1)e^{-i\beta_1} & \cosh(S_1)e^{-i\alpha_1} \end{pmatrix}. \quad (18)$$

In a semiclassical theory we have

$$\alpha_1 = - \int_{x_1}^{x'_1} k(x)dx - \int_{x'_1}^{x_2} k(x)dx, \quad (19)$$

$$\beta_1 = \frac{\pi}{2} - \int_{x_1}^{x'_1} k(x)dx + \int_{x''_1}^{x_2} k(x)dx. \quad (20)$$

$S_1$  characterizes the height of the potential, as the transmission coefficient  $t_1$  is given by  $t_1 = e^{i\alpha_1} \text{sech} S_1$ . Because we assume that the peak is high, which means  $S_1 \gg 1$ . The transmission probability  $|t_1|^2$  is then approximated as  $|t_1|^2 \sim 4e^{-2S_1} \ll 1$ .

Similarly, we introduce the transfer matrix for the second peak as

$$\begin{pmatrix} A_2 \\ B_2 \end{pmatrix} = \Theta_2 \begin{pmatrix} A_3 \\ B_3 \end{pmatrix}, \quad (21)$$

and we have

$$\Theta_2 = \left(\frac{k_3}{k_2}\right)^{\frac{1}{2}} \begin{pmatrix} \cosh(S_2)e^{i\alpha_2} & \sinh(S_2)e^{i\beta_2} \\ \sinh(S_2)e^{-i\beta_2} & \cosh(S_2)e^{-i\alpha_2} \end{pmatrix}. \quad (22)$$

The phases  $\alpha_2$  and  $\beta_2$  can be written similarly to  $\alpha_1$  and  $\beta_1$ , where  $S_2 \gg 1$ . We assume that  $S_i$ ,  $\alpha_i$ , and  $\beta_i$  ( $i = 1, 2$ ) are smooth functions of the parameters  $Q_1$ ,  $Q_2$  and  $E_F$ . A transfer matrix  $\Theta$  for the entire system is given by

$$\Theta = \Theta_1 \Theta_2 = \left(\frac{k_3}{k_1}\right)^{\frac{1}{2}} \begin{pmatrix} \theta_{11} & \theta_{21}^* \\ \theta_{21} & \theta_{11}^* \end{pmatrix}, \quad (23)$$

$$\theta_{11} = e^{i(\alpha_1 + \alpha_2)} (\cosh S_1 \cosh S_2 + \sinh S_1 \sinh S_2 e^{i\omega}), \quad (24)$$

$$\theta_{21} = e^{i(\alpha_2 - \beta_1)} (\sinh S_1 \cosh S_2 + \cosh S_1 \sinh S_2 e^{i\omega}), \quad (25)$$

$$\omega = \beta_1 - \beta_2 - \alpha_1 - \alpha_2 \cong 2 \int_{x_1'}^{x_2'} k(x) dx. \quad (26)$$

From unitarity, it follows that  $|\theta_{11}|^2 - |\theta_{21}|^2 = 1$ . We assume that the Fermi energies of the two leads are identical, which means  $k_3 = k_1$ . For a plane wave incident from the left lead, let  $r$  and  $t$  denote the reflection and transmission coefficients, respectively. Similarly, for a plane wave from the right lead, we define  $r'$  and  $t'$  as well. We then obtain

$$r = \theta_{21}/\theta_{11}, \quad t = t' = 1/\theta_{11}, \quad r' = -\theta_{21}^*/\theta_{11}. \quad (27)$$

It implies the unitarity  $|r|^2 = |r'|^2 = 1 - |t|^2$ . It also satisfies  $t = t'$  and  $rt^* + r'^*t = 0$ , as is required from time-reversal symmetry.

We now apply this framework to fit our numerical results. Because  $r$  is written as

$$r = e^{i\theta} \frac{\tanh S_1 + \tanh S_2 e^{i\omega}}{1 + \tanh S_1 \tanh S_2 e^{i\omega}}, \quad (28)$$

a condition for a total transmission,  $r = 0$ , is given by

$$S_1 = S_2, \quad (29)$$

$$\omega = 2 \int_{x_1'}^{x_2'} k(x) dx = (2n + 1)\pi, \quad (30)$$

where  $n$  is an integer. The latter condition is equivalent to the Bohr quantization condition, that the state localized around  $x_2$  be an eigenstate with its eigenenergy equal to  $E_F$ . In other words the total transmission occurs at resonance. For fixed  $E_F$ , the two conditions (29) and (30) define isolated points in the  $Q_1$ - $Q_2$  plane. Let  $P$  denote one of such points of total transmission:  $r = 0$ . One can easily see that around the point  $P$ , the phase of  $r$  and that of  $r'$  wind by  $\pm 2\pi$ , as is schematically shown in Fig. 7(a1) (a2). As is seen from the Brouwer formula (13), the phase windings of  $r$  and  $r'$  correspond to ( $2\pi$

times) the amount of charge pumped into the system through the left and the right ends, respectively. Thus, by going around the point  $P$ , one unit charge is pumped from the left lead to the right. For illustration, let us consider a clockwise cycle around the point  $P$  in Fig. 7 (a1)(a2). This pumping from left to right is analogous to the “bicycle pump” [28]. The two potential peaks correspond to two gates to control the pumping. If the system crosses the line  $\omega = (2n + 1)\pi$  at the  $S_1 < S_2$  side,  $r$  undergoes  $2\pi$  phase changes. It means that tunneling occurs through the left potential peak due to resonance, corresponding to the opening of a “left gate” and a unit charge flows in. After that the left gate closes, and the right gate opens in turn, when the system crosses the line  $\omega = (2n + 1)\pi$  at the  $S_1 < S_2$  side, and  $r'$  undergoes  $-2\pi$  phase change. The charge is pumped to the right lead after one cycle. Thus the overall motion of the charge is as shown in Fig. 7 (a3). For the pumped charge to be quantized, the cyclic process should be sufficiently slow to be regarded as “adiabatic”. Otherwise the particle cannot tunnel through the potential barriers. Below let us make this physical picture more explicit in relation to our numerical results.

In our numerical results in Fig. 3(b2)-(b4), the phase-winding point  $P$  corresponds to the perfect transmission. When we go from Fig. 3(b2) to (b4),  $L/\xi$  increases. In the resonance-tunnelling picture, it means that  $S_i$  increases and that the “resonance-tunnelling wing” narrows, as is seen by comparing Fig. 7(a1) and (b1). It is exactly observed in our numerical results.

For large  $L/\xi$ , the transmission probability  $|t|^2$  is typically  $\sim e^{-2(S_1 + S_2)} \sim e^{-2L/\xi}$ . Because we have  $S_1 \sim S_2$  near the resonance, we estimate  $S_1 \sim S_2 \sim (L/2\xi)$ . In that case, the change of the phases of  $r$  and  $r'$  occurs abruptly at around  $|\omega - (2n + 1)\pi| \sim e^{-L/\xi}$ . Along the line  $\omega = (2n + 1)\pi$ ,  $|r|$  is given by  $|r| = \tanh(S_1 - S_2)$ , which becomes appreciable only when  $|S_1 - S_2| \sim 1$ . This is found only in a small region  $\Delta/t_{\text{n.n.}} \sim \xi/L$ . When  $L/\xi \gg 1$ , because the tunnelling rate  $Q_W$  is exponentially small ( $Q_W \sim t_{\text{n.n.}} e^{-L/\xi}$ ), charge pumping requires an exponentially long time  $\tau \sim (\hbar/t_{\text{n.n.}}) e^{L/\xi}$ . This is a time scale which gives a criterion for adiabatic charge pumping in this system. If one changes the parameters faster than this time scale, the pumped charge is reduced with an exponential factor  $e^{-\omega/E_G}$  as a nonadiabatic correction, where  $\omega$  is a frequency of the change the external parameters [34].

Generally, there occurs no perfect transmittance point by tuning only two parameters since the effective two barrier model for the resonant tunnelling applies only to a limited region of the random system and not through a whole sample. In the present case it is guaranteed by the topological constraint that the phase of  $r$  ( $r'$ ) should wind by  $(- )2\pi$  for a large cycle far from  $\vec{Q} = 0$ , well within the gapped region [9]. When  $|\vec{Q}|$  is larger than the



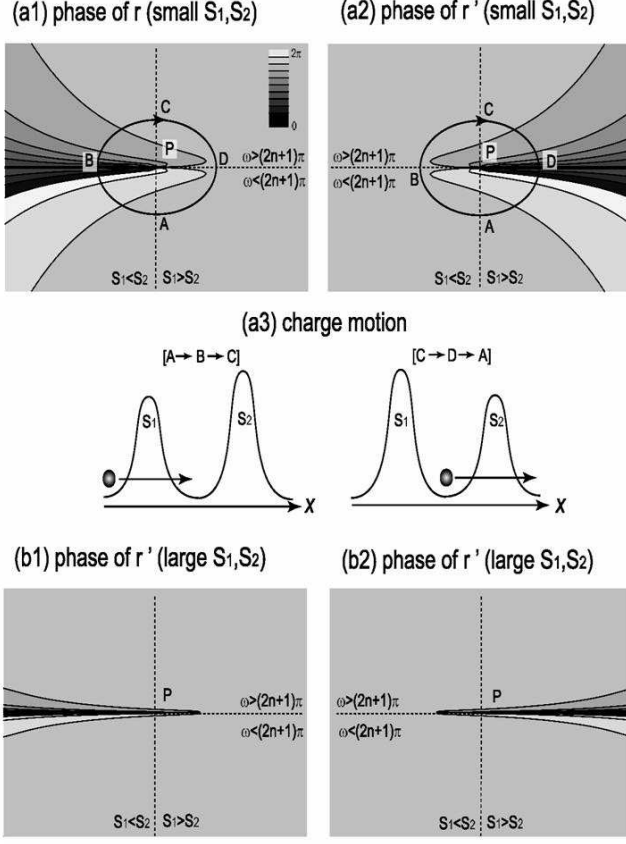


FIG. 7: Schematic contour mapping of the phases of the reflection coefficients  $r$  and  $r'$  in the  $Q_1$ - $Q_2$  plane. (a1)(a2) correspond to small  $S_1$ ,  $S_2$ , and (b1)(b2) to large  $S_1$ ,  $S_2$ . The phases of  $r$  and  $r'$  wind by  $2\pi$  during the cycle around the “vortex”  $P$ . When we go along the arrows indicated in the figures (a1)(a2), the phase of  $r$  ( $r'$ ) increase by  $2\pi$  ( $-2\pi$ ). (a3) illustrates the motion of the charge in the cycle. Note that the  $2\pi$  phase change of  $r$  ( $r'$ ) is associated with pumping one unit charge into the system through the left (right) end of the system.

energy scale of the disorder, a finite gap ( $\sim |\vec{Q}|$ ) opens. The wing will then become as wide as  $Q_W \sim |\vec{Q}|$ . Correspondingly, the typical time scale  $\tau \sim \hbar/Q_W \sim \hbar/|\vec{Q}|$  becomes smaller, and the adiabaticity condition is easily satisfied. In such case, however, the dielectric response is not enhanced. The localization length becomes as long as the system size, and the pumping is accomplished through extended states, not by resonance tunnelling. Remarkably, this charge pumping in the gapped region is governed by the vortex which is located deep in the disordered regime ( $\xi \ll L$ ). In other words, the charge pumping in the gapped regime ( $\xi \sim L$ ) is smoothly connected to that via resonance tunnelling in the disordered regime ( $\xi \ll L$ ). We note that  $S_1$  and  $S_2$  are regarded as effective parameters, although the real potential is much more complicated than the two-barrier structure.

### Multi-channel problem in alloy model for on-site random potential

In the rest of this section, we consider a stronger randomness by employing the alloy model (Fig. 2 (b)) with  $v_i = s_i(v + \delta v_i)$  with  $s_i = \pm 1$  being a random sign and  $\delta v_i/v \in [-0.025, 0.025]$  a uniform random distribution, instead of the uniformly distributed random potential (Fig. 2 (a)).

Let us start with the single-channel case. Then, for a fixed disorder strength  $v$ , the shape of the vortex core of the reflection coefficient rapidly evolves from isotropic to anisotropic with increasing the system size  $L$ , as in the case of the uniformly distributed random potential discussed in Sec . This tendency is generic and also realized for a fixed system size  $L$  with increasing the disorder strength  $v$ . In Figs. 8 (a) and (b), we show the reflectance  $R$  and the phase  $\varphi$  in the  $\vec{Q}$  space for  $v/t_{n.n.} = 1.0$  and a small sample size  $L = 25$ . Here, the region in the  $\vec{Q}$  plane where the gap collapses and vortices distribute expands because of the stronger disorder and thus the much shorter localization length  $\xi \sim 3$  or 4. The transmittance  $T$  is typically obtained as  $\sim 10^{-9}$ , which is practically negligible except at the vortex core.

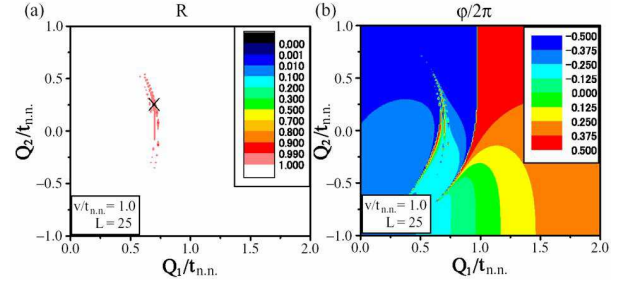


FIG. 8: (a) Reflectance and (b) the phase  $\varphi$  of  $r$  in disordered system with  $L = 25$  and  $v/t_{n.n.} = 1.0$  for the alloy model with the on-site random potential given by Fig. 2.

Now we consider a system that consists of many channels, each of which is described by the present disordered alloy model but with a different profile of random potentials. Such configuration can be realized in thin films of ferroelectrics. Then, we can design the pattern of the phase  $\varphi$  in the  $\vec{Q}$  plane by tuning the disorder. For the alloy model with the random on-site potentials, vortices are mostly located around  $Q_1 = \pm v/2$  with the “wing” almost along the  $Q_2$  axis. Therefore, we can enhance the dielectric response, if we can tune the disorder strength and choose a sample where the  $\vec{Q}$  point of



the system is located inside the “wing”. In particular, when the transmittance  $T$  is negligibly small, the enhancement factor of the dielectric response is given by  $(\partial\varphi/\partial\theta)_{\text{disorder}}/(\partial\varphi/\partial\theta)_{\text{pure}}$  from (13), since the electric field is proportional to  $\theta = \arctan(Q_1/Q_2)$ . We calculate this enhancement factor for this multichannel system. Increasing the number  $N$  of channels. Figures 9(a) and (b) represent the  $\bar{Q}$  dependence of the enhancement factor in the case of  $v/t_{\text{n.n.}} = 1.6$  and 2.4, respectively, for  $L = 25$  with  $N = 102$ . The main structure in this map is almost saturated up to  $N = 10^2$ . These results reveal that around  $Q_1 \sim \pm v/2$ , the dielectric response is significantly enhanced by a factor  $30 \sim 40$  compared with the pure case. Even for the thin film with a square shape of a linear dimension larger than  $50\text{\AA}$ , which corresponds to  $N = 10^2$ , the disorder-induced enhancement of the charge transfer rate should be robust. Then, the applied electric field necessary for switching the polarization is reduced by this enhancement factor. If we require the response time  $\tau \sim e^{L/\xi}/t_{\text{n.n.}}$  of the order of  $10^{-9}$  s, we obtain  $e^{L/\xi} < 10^6$  with the assumption of  $t_{\text{n.n.}} \sim 10^{15} \text{ s}^{-1}$ . This also assures a negligibly small transmittance  $T \sim e^{-L/\xi} \sim 10^{-6}$ , and thus the small leak current and low dissipation.

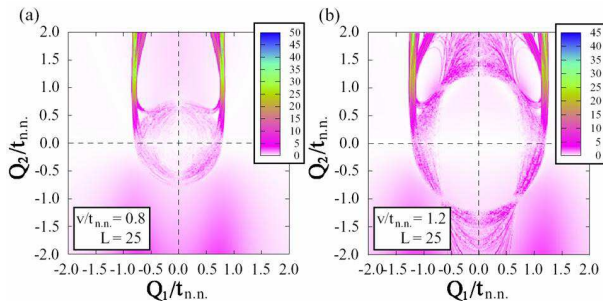


FIG. 9: Relative dielectric response in the presence of the disorder compared with the pure case. The disorder strength is  $v/t_{\text{n.n.}} = 0.8$  for (a) and 1.2 for (b). Averages are taken over  $10^2$  random disorder configurations. Inside white bands, there occurs a gradual sign change in the dielectric response.

Possible experimental realization of this quantum-mechanical disorder-induced enhancement of the dielectric response, namely the quantum relaxor, has also been proposed [10] for thin films of solid solution systems like  $\text{Pb}(\text{Fe}_{0.5}\text{Nb}_{0.5})\text{O}_3$  and  $\text{Pb}(\text{Sc}_{0.5}\text{Nb}_{0.5})\text{O}_3$  prepared with an adequate slow-anneal process [35, 36].

## PERIODIC/TWISTED BOUNDARY CONDITION

The adiabatic charge pumping in the presence of the substrate disorder was considered by Niu *et al.*[9]. They showed that the adiabatic charge transport is still quantized as long as the excitation gap between the highest occupied state (HOMO) and lowest unoccupied state (LUMO) does not vanish due to the substrate disorder and the many-body interaction in the thermodynamic limit. In the case of open boundary condition, it is easy to imagine the meaning of the charge pumping, namely the charge transport from one end to the other. In the case of periodic boundary condition, the charge pumping after one-cycle means that the electronic wavefunction shifts by the minimum number of lattice sites so that the final wavefunction is the same as the initial one. A cartoon picture of this process is given by Fig. 10. We note that in the absence of the disorder, the adiabatic charge transport has been related to the field-theoretical model of the one-dimensional chiral anomaly[37].

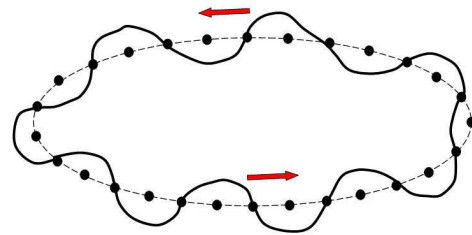


FIG. 10: A cartoon picture of the charge transport on the one-dimensional ring.

## Formalism

We consider a one-dimensional charge-density-wave system with disorder, as described in (3) and (7). In contrast to the open system with two leads as considered in Section III, we deal with a closed system in a ring geometry. Instead of a periodic boundary condition as is usually employed for the ring, we introduce a twisted boundary condition; we impose that the phase gained by running around the ring once is  $e^{i\alpha}$ . This twisted boundary condition is realized by applying a magnetic flux through the one-dimensional ring.

The reason for introducing the twisted boundary condition is to reveal the topological nature of the charge transport in the system. In the pure case, the lattice

momentum  $k$  is a good quantum number, and the topological nature is manifest in the three-dimensional space  $(Q_1, Q_2, k)$  as monopoles and antimonopoles. However,  $k$  is no longer a good quantum number in the disordered case, and instead the flux  $\alpha$  plays a similar role to  $k$ . Therefore, instead of  $(Q_1, Q_2, k)$ , we will be interested in the adiabatic process such that the system is changed due to the slow variations of the parameters  $(Q_1, Q_2, \alpha)$ , which spans a 3-dimensional parameter space with the property  $\alpha \in [0, 2\pi]$ . The Hamiltonian with the flux  $\alpha$  can be rewritten as

$$\begin{aligned} H(\alpha) = & -\frac{t_{\text{n.n.}}}{2} \sum_{j=1}^N (e^{i\alpha/N} c_j^\dagger c_{j+1} + h.c.) \\ & + Q_1 \sum_{j=1}^N (-1)^j c_j^\dagger c_j \\ & + \frac{Q_2}{2} \sum_{j=1}^N (-1)^j (e^{i\alpha/N} c_j^\dagger c_{j+1} + h.c.) + V \end{aligned} \quad (31)$$

where  $c_{N+1} \equiv c_1$  and  $V = \sum_j v_j c_j^\dagger c_j$  is the uniformly distributed disorder potential.

In the tight binding model, the polarization operator  $\vec{P}$  has the following form

$$\vec{P} = \sum_j \vec{R}_j c_j^\dagger c_j \quad (32)$$

where  $\vec{R}_j$  is the position at site  $j$  and  $c_j^\dagger c_j$  is the electron density operator. The current is defined as the time derivative of the polarization operator given by

$$\vec{J} = \frac{\partial \vec{P}}{\partial t} = \frac{1}{i} [\vec{P}, H] \quad (33)$$

In the pure case the current is given by  $\frac{\partial H}{\partial k}$ , whereas in the present case with disorder, the current operator given by  $\frac{\partial H}{\partial \alpha}$  has the following form

$$J = ie^{-i\alpha/N} \sum_j (t + Q_2(-1)^j) c_{j+1}^\dagger c_j + h.c. \quad (34)$$

When the flux  $\alpha$  is equal to 0 or  $\pi$ , the system is time-reversal symmetric, and there is no persistent current. In such cases, we can consider a change of the electric polarization by an adiabatic change of parameters  $Q_1$  and  $Q_2$ . In the linear response theory, the change of the electric polarization is given by

$$\delta P = F_1 \Delta Q_2 - F_2 \Delta Q_1, \quad (35)$$

with

$$F_1 = -\frac{i}{L} \sum_{m \neq 0} \left( \frac{\langle \Psi_0 | J | \Psi_m \rangle \langle \Psi_m | \frac{\partial H}{\partial Q_2} | \Psi_0 \rangle}{(E_m - E_0)^2} - c.c. \right), \quad (36)$$

$$F_2 = \frac{i}{L} \sum_{m \neq 0} \left( \frac{\langle \Psi_0 | J | \Psi_m \rangle \langle \Psi_m | \frac{\partial H}{\partial Q_1} | \Psi_0 \rangle}{(E_m - E_0)^2} - c.c. \right), \quad (37)$$

where  $L = Na$  is the circumference of the ring, and  $a$  is the lattice spacing, and

$$\begin{aligned} \frac{\partial H}{\partial Q_1} &= \sum_j (-1)^j c_j^\dagger c_j \\ \frac{\partial H}{\partial Q_2} &= \frac{1}{2} \sum_j (-1)^j (e^{i\alpha/N} c_j^\dagger c_{j+1} + e^{-i\alpha/N} c_{j+1}^\dagger c_j) \end{aligned} \quad (38)$$

We note that the change of the polarization,  $\delta P$ , is in general dependent on the path in the parameter  $(\vec{Q})$  space. The  $|\Psi_0\rangle$  in (36) and (37) is the many-body ground state, and  $|\Psi_m\rangle$  denote the excited states.  $E_0$  and  $E_m$  are the energy for the ground and the excited states, respectively. In the pure case when the chemical potential lies in the gap, the system is a band insulator. The magnitude of the energy gap is given by the magnitude of the CDW order parameter  $(Q_1, Q_2)$ . In the presence of the disorder, the gap closes when the magnitude of the disorder potential becomes the order of  $\mathcal{O}(\sqrt{Q_1^2 + Q_2^2})$ . The system remains insulating because each state is localized, i.e., Anderson localization.

Although we have defined (35), (37) and (36) only for  $\alpha = 0$  and  $\alpha = \pi$ , we henceforth extend these formulae to general  $\alpha$ , which makes the topological properties of the charge pumping manifest. We note that except for  $\alpha = 0$  and  $\pi$ ,  $\delta P(\alpha)$  does not mean a change of polarization. With this extension to arbitrary  $\alpha$ , let us succinctly abbreviate  $(Q_1, Q_2, \alpha)$  as  $\vec{Q} = (Q_1, Q_2, Q_3)$  and define the gauge potential as

$$\vec{A} = i \langle \Psi_0 | \frac{\partial}{\partial \vec{Q}} | \Psi_0 \rangle. \quad (40)$$

This gauge field is so defined that the corresponding field strength  $\vec{F} = \nabla \times \vec{A}$  has the components given in (37) and (36). Furthermore, when the parameters  $(Q_1, Q_2)$  are changed along a cycle, the pumped charge can be written as

$$\delta P(\alpha) = \oint_S d\vec{Q} \times \hat{\alpha} \cdot \vec{F}(\vec{Q}) \quad (41)$$

where  $S$  is a loop on the  $Q_1$ - $Q_2$  plane. Using the Stoke's theorem, (41) becomes

$$\delta P(\alpha) = \int d^2 Q D(\vec{Q}) \quad (42)$$

where  $D(\vec{Q}) = \partial_1 F_1 + \partial_2 F_2$  defined as the distribution function of the polarization. This pumped charge is not necessarily an integer.

Nevertheless, in a strongly disordered system it becomes an integer, with an exponentially small correction of the order of  $e^{-L/\xi}$ . To see this, we note that the wavefunctions in a strongly localized case are almost intact with the twisted boundary condition  $\alpha$  within an

accuracy of  $e^{-L/\xi}$ . Hence  $\Delta P(\alpha)$  is equal to an average  $\Delta P(\alpha)$  over  $\alpha$ , namely

$$\Delta P = \int_0^{2\pi} \frac{d\alpha}{2\pi} \Delta P(\alpha) = \int_{\partial T} d\vec{\sigma} \cdot \vec{F} \quad (43)$$

where  $\partial T$  is the torus surface, and  $d\vec{\sigma}$  is the surface element. This average  $\Delta P$  represents the total flux over a torus surface, and it is an integer, which follows from topological properties of the gauge field  $\vec{A}$ . As the field strength is defined as  $\vec{F} = \nabla \times \vec{A}$ , it satisfies  $\nabla \cdot \vec{F} = 0$  if there is no singularity, i.e. there is no energy crossing. Thus when there are no energy degeneracies inside the torus  $V \times [0, 2\pi]$ , the averaged pumped charge  $\Delta P$  becomes zero due to the Gauss theorem. If there is a energy crossing, the gauge field  $\vec{A}$  has a U(1) monopole there, and the averaged charge  $\Delta P$  becomes a total strength of the monopoles inside the torus, again by using the Gauss theorem. As the monopole strength is quantized to be an integer,  $\Delta P$  is always an integer. This discussion for (43) corresponds to that for (2.23) in Ref. 9, in which they claimed that the charge transport is quantized in the presence of gap which does not vanish in the thermodynamic limit. On the other hand, the aim of this paper targets at another respect: we are interested in the strong disorder case, in which the energy gap closes in the thermodynamic limit and all wave functions are localized characterized by the localization length  $\xi$  defined by  $\xi^{-1} = \int dx |\psi(x)|^4$ , where  $\psi$  is the single particle wave function. Nevertheless, for finite-sized systems gap always exists which is the order of the band width divided by the size of the system, which validates the above topological argument even in the strongly disordered cases. In such disordered systems, the field strength  $\vec{F}$  is highly anisotropic around the monopoles, which is closely related with a “resonance tunnelling” picture in section III.B as we explain in the next paragraph.

The adiabatic charge transfer is based on the occurrence of the singularity in the parameter space[6], which happens when LUMO and HOMO are degenerate. By making a close contour enclosing the singularity, the wave function shifts as shown in Fig. 10. Since the disorder potential is random, we expect that the proliferation of the singularities may occur. Furthermore, there could be *singularity string* rather than *point* in the strong disorder limit. The reason is given as the following. In the strong disorder limit, all wave functions are localized. There could be a situation that the wave function of the LUMO and the HOMO are well separated so that the overlap integral of two wavefunctions are exponentially small as the parameters change. Thus even when the change of parameters in numerics or in experiments is very slow, its timescale might be still shorter than the inverse of the (exponentially small) overlap integral of the LUMO and HOMO. Therefore, within this variation of parameters, the LUMO and HOMO can be regarded as degenerate. Once they are degenerate at a certain point in the pa-

rameter space, they will keep the near-degeneracy as the parameters change until their wave functions have appreciable overlap and open a gap. As long as they remain nearly degenerate as the parameters change, the singularity string is created in the parameter space. Moreover, because the wave functions are highly localized on the singularity string, they are *insensitive to the boundary condition*, in other words,  $\alpha$ -independent. Therefore, they have the sheet-like structure extending along the  $\alpha$ -direction in the parameter space. Even though it is sheet-like, we call it a string referring to its projection on the  $(Q_1, Q_2)$  plane. From this observation, we conclude that the singularity in the parameter space projected on  $Q_1$  and  $Q_2$  subspace has two kinds, points and strings, in the strong disorder limit. The former contribute to the charge transfer, while the latter do not. The charge transfer for the former is explained within the resonance tunnelling Section .

## Numerical Result

In this section, we solve numerically the eigenvalue problem for slowly varying parameters  $(Q_1, Q_2)$  and calculate the contour integral in (41). We introduce the small segment  $\Delta\vec{Q}$  for the contour integral, and demand that  $F_1, F_2$  are continuous. Therefore, the size  $|\Delta\vec{Q}|$  determines the energy-scale and time-scale of our simulation. In actual calculation, we take  $|\Delta\vec{Q}| = 10^{-6}t_{n.n.}$  as the finest one. Then the discussion below applies when we observe the system within the time-scale  $T \sim \hbar/|\Delta\vec{Q}| \sim 10^6\hbar/t_{n.n.}$ . Also we average over  $\alpha$  to see the quantization of the charge transfer in (43).

We solve (31) by a direct numerical calculation. Our goal is to compute the distribution function from the (42), which is  $\alpha$ -dependent. We will also demonstrate the quantization of the charge transfer by averaging over  $\alpha$  by (43).

We consider a ring with  $N = 50$  and take  $v_i/t_{n.n.}$  to distributes uniformly in  $[-7.0, 7.0]$ . To obtain the distribution function, we divide the  $(Q_1, Q_2)$  plane into small pieces of grids and calculate (42) for each grid. Let us remind the readers that the distribution function for the pure case is the  $\delta$ -function at the origin[6]. In that case, we do not need to integrate over  $\alpha$  to obtain the quantization of the charge transfer, because the singularity lives in the  $(Q_1, Q_2, k)$  space, and the integration over  $k$  is already included implicitly in (42).

Our result can be summarized by the cartoon in Fig. 11. First, we found that  $\Delta P = 1.0$  if we take the loop **A** which is the outer dash one ( $|\vec{Q}| \sim 10$ ) and average over  $\alpha$ . It corresponds to the weak disorder case where the strength of the disorder is much smaller than  $|\vec{Q}|$ , so the potential strength is not large enough to close the gap. According to Niu and Thouless[9], the polarization is quantized, and we reproduce their result

here. Secondly, the singularity strings appear in the region  $|\vec{Q}| \leq 4.5$ . In this region, the disorder potential is strong enough to close the gap. As we pointed out in the section, there are two kinds of the singularities, points and strings. In the "stringful" region, it is rather difficult to locate the singularity *point*. It is because the operation of the adiabatic process changes when making the contour across a string. In Fig. 12, we illustrate two different adiabatic processes regarding making contours enclosing the singularity points and across the singularity string. Fig. 12(a) shows the usual definition of the adiabatic process. In the presence of the gap, the adiabatic process has to follow the lower energy state, which is indicated by the square dots in Fig. 12(a). Fig. 12(b) shows the adiabatic process of the contour across the string. In this case, because the wave functions of the HOMO and the LUMO do not overlap, the adiabatic process needs to keep ramping up to the higher energy state at the first degenerate point and ramp down to the lower energy state at a second degenerate point, which completes a close loop. Note that the energy of the HOMO is larger than that of the LUMO after the first degenerate point and becomes smaller again after the second degenerate point. In other words, the system stays in the same state, and thus the charge does not transfer at all after a close contour. Therefore, even if we make a close loop which encloses a whole singularity string, the charge does not transfer. It should be noted that even though the system is at a higher energy state, it takes  $\sim eL/\xi$  to relax, where  $L$  is the size of the system, and  $\xi$  is the typical localization length which is around 3 sites in our case.

In Fig. 12(c), we demonstrate a real process across a singularity string indicated by the loop **C** in Fig. 11. Usually, we refer singularity string to the degenerate manifold between the HOMO and LUMO. In a real process, we may have to consider the degeneracy between the HOMO and the 2<sup>nd</sup> LUMO. For example, after the degenerate point between LUMO and HOMO, the descending order in energy is 2<sup>nd</sup> LUMO, HOMO, and the LUMO. There is the possibility, for example the boundary  $\beta$  in Fig. 12(c), that the energy of 2<sup>nd</sup> LUMO and that of HOMO can be the same along the contour before meeting the next degenerate point between HOMO and LUMO. If it happens, the system still stays in the original HOMO state by ramping further up to the higher energy state. After that, the descending order in energy becomes HOMO, 2<sup>nd</sup> LUMO, and LUMO. Fig. 12(c) shows the complete process and the system has to go back to its original state after completing a close loop. As a result, HOMO, LUMO, and other states can be viewed as the Riemann sheets. Singularity strings are like the branch cuts which connect different Riemann sheets. Contours on the  $(Q_1, Q_2)$  plane are very similar to the one in the complex plane.

As the string just corresponds to the degenerate states which does not penetrate through the whole sample, the only topological object which contributes to the po-

larization is the isolated singularity *point*. We found one at  $(Q_1, Q_2, \alpha) = (-0.3885, -4.80415, 0)$ . If we calculate (43) around that point, for example loop **B** in Fig. 11, we obtain  $\Delta P = -1.0$ . We identify the singularity point which carries  $\Delta P = -1.0$  with the antimonopole in contrast to the monopole which carries  $\Delta P = 1.0$ . Considering together with the total flux calculated from the loop **A** in Fig. 11 to be 1.0, *there must be at least two monopoles and one antimonopole in our system, which demonstrates the proliferation of the monopole-antimonopole pairs in the strong disorder limit*. Unfortunately, we are not able to locate monopoles exactly but obtain rough position, since they merge in the stringful soup. The integral in (41) converges very slowly as the counters are close to the singularity string (or points). The integral step is equivalent to the rate of the adiabatic process, which has to be less than the typical energy spacing  $2(t + v_i^{\max})/N$ . When approaching to the singularity, the energy gap becomes very small, so the process rate has to be smaller to have convergent result. Therefore, it is very difficult to locate the monopole position if they are in the stringful soup.

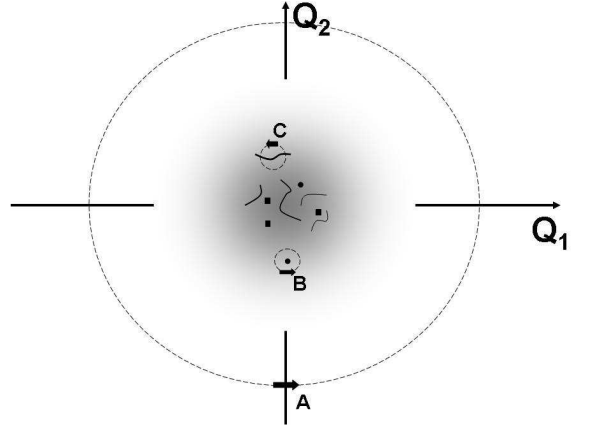


FIG. 11: A cartoon picture of the distribution of singularities at  $\alpha = 0$ . The singularity has two kinds: strings and points. Calculating (41) from the outer big dash loop gives the polarization  $+1.0$  and  $-1.0$  from the loop **B**. If we stay far away from the origin, one would think that there is only one monopole with  $\Delta P = 1.0$  at the center like the pure case. However, when the disorder strength is strong enough, there are some subtle structure inside the big monopole. There are the monopole-antimonopole pairs and the singularity strings.

The appearance of the antimonopoles in the strong disorder limit is very appealing. It contributes to the polarization in the opposite way to that a monopole does. The polarization comes from the charge transportation through the whole sample from one end to the other. Therefore, (42) for the antimonopole must be highly  $\alpha$ -dependent shown in the Fig. 13(a). The peak value of  $\Delta P(\alpha)$  happens at  $\alpha = 0$ . After integrating over  $\alpha$  by (43), we obtained  $\Delta P = -1.0$ . This result indicates that

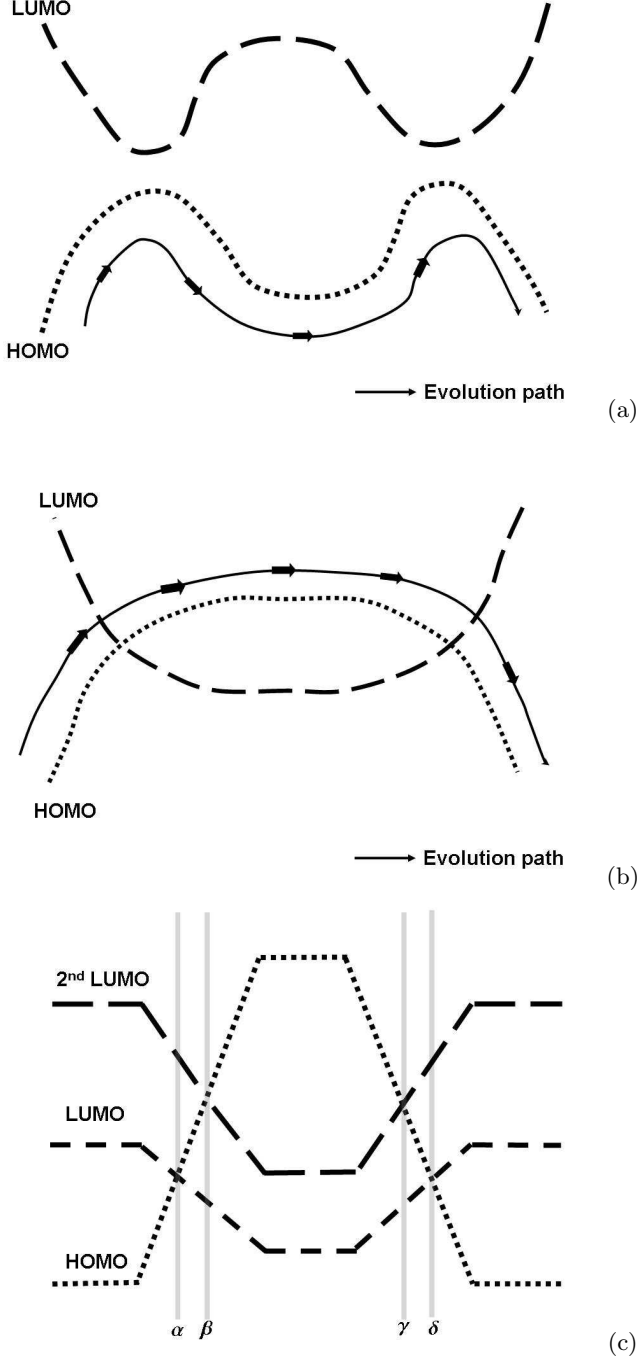


FIG. 12: The adiabatic process in the gapless case is different from the gap case. (a) shows the process with a gap. (b) shows the process without a gap. (c) a real process from loop C in the Fig. 11.

the antimonopole may be located at  $\alpha = 0$ . In Fig. 13(b), we found that the energy gap closes at  $\alpha = 0$  supporting this observation. In Fig. 13(c) and 13(d), we show the energy gap at  $\alpha = 0$  along  $Q_1$  and  $Q_2$  direction, respectively. In fact, the structure of the antimonopole is highly anisotropic. The energy gap has a valley-like structure at

$\alpha = 0$ . Fig. 13(e) shows the energy gap along the valley. The slope of the energy gap function along the valley is roughly 10 times smaller than other directions. In other words, the antimonopole looks like a football more than a round ball. This anisotropy can be understood in terms of the resonance tunnelling as we see in the next section.

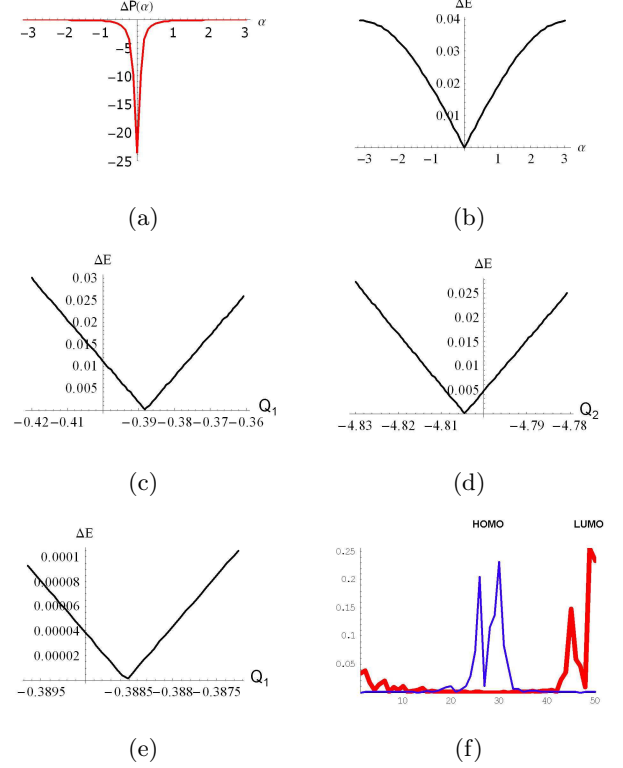


FIG. 13: Some properties of antimonopole. (a) the  $\alpha$ -dependence of (42) around the antimonopole. (b), (c), and (d) the energy gap functions of the antimonopole along the  $\alpha$ ,  $Q_1$ , and  $Q_2$  direction. (e) the gap function along the valley. The antimonopole is not spherically symmetric. The gap function at  $\alpha = 0$  has a deep valley because the slopes along the valley is 10 times smaller than other directions. (f) The wave functions of the HOMO and LUMO at the antimonopole. In Figs. (b)-(e) the axes are in the unit of  $t_{n,n..}$ .

Another quantity to measure the extendedness of a state is the Thouless number defined by

$$\mathcal{N}_T = \frac{E(\alpha = \pi) - E(\alpha = 0)}{\delta E} \quad (44)$$

where  $E(\alpha)$  is the energy of the state and  $\delta E$  is the typical energy spacing. We plot the Thouless number of the HOMO in Fig. 14. We found a ridge distribution which coincides with the valley in the energy gap function. The antimonopole locates at the ridge but not necessarily the highest one. The Thouless number at the ridge is one order of magnitude larger than the other points in the vicinity in the parameter space. It suggests that the high boundary condition sensitivity must dominate the

physics at the antimonopole. It leads to the resonance tunnelling in the Anderson insulator.[33]

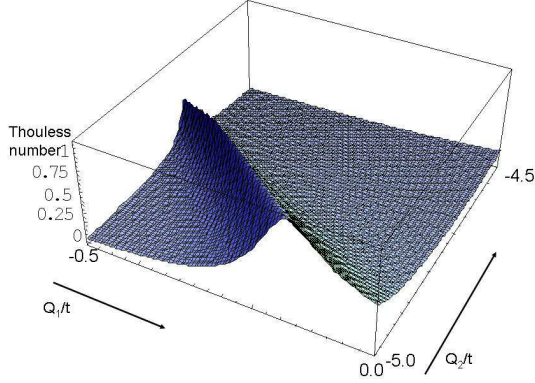


FIG. 14: The Thouless number in the vicinity of the antimonopole. The Thouless number has a ridge structure which exactly coincides with the valley in the gap function.

### Resonance Tunnelling

We now compare the numerical results with the picture of resonance tunnelling discussed in Sec. . In the resonance tunnelling scenario, we can deal with the periodic system by identifying  $x_3$  with  $x_1$ . It leads to  $k_3 = k_1$ . In such a periodic system, as is apart from an open system,  $E_F$  is no longer a tunable parameter, but corresponds to discrete energy levels of the system. Thus,  $S_i$ ,  $\alpha_i$ , and  $\beta_i$  are smooth functions of  $Q_1$ ,  $Q_2$  and an energy  $E$ . Because the periodic system is threaded by a flux of  $\alpha\Phi_0$ , we require that

$$\Theta \begin{pmatrix} A_3 \\ B_3 \end{pmatrix} = \begin{pmatrix} A_1 \\ B_1 \end{pmatrix} = e^{i\alpha} \begin{pmatrix} A_3 \\ B_3 \end{pmatrix}. \quad (45)$$

It yields  $\det(\Theta - e^{i\alpha}) = 0$ , i.e.  $\text{Re}\theta_{11} = \cos\alpha$ . Because  $\theta_{11}$  is a function of  $Q_1$ ,  $Q_2$  and  $E$ , this defines a (discrete) energy level of the system as a function of  $Q_1$  and  $Q_2$ .

We study the monopoles in the framework of resonance tunnelling. As the monopoles appear at band-crossing points, we have to look for degenerate solutions of (45). Namely, we look for cases with two (degenerate) states for fixed  $Q_1$ ,  $Q_2$  and  $E$ . This happens if and only if the matrix  $\Theta$  is equal to  $e^{i\alpha}$ . This condition reduces to

$$S_1 = S_2, \quad (46)$$

$$\omega \cong 2 \int_{x_1''}^{x_2'} k(x) dx = (2n+1)\pi, \quad (47)$$

$$\omega' \cong 2 \int_{x_2''}^{x_3} k(x) dx + 2 \int_{x_1}^{x_1'} k(x) dx = (2n'+1)\pi,$$

$$\alpha = -(n + n' + 1)\pi, \quad (48)$$

$$\alpha = -(n + n' + 1)\pi, \quad (49)$$

where  $n$  and  $n'$  are integers. Because  $S_1$ ,  $S_2$ ,  $\omega$  and  $\omega'$  are functions of  $Q_1$ ,  $Q_2$  and  $E$ , the three conditions (46), (47) and (48) determine a set of isolated points in the  $Q_1$ - $Q_2$ - $E$  space. Combining with (49), we get isolated points in the  $Q_1$ - $Q_2$ - $\alpha$  space, corresponding to the monopoles/antimonopoles [38]. Except for the vicinity of the monopoles/antimonopoles, the field  $\vec{F}$  is almost  $\alpha$ -independent, because the system is almost intact with the change of  $\alpha$ . Thus the distribution of the field  $\vec{F}$  is as shown in Fig. 15(a). In contrast with a small-sized model  $\xi \sim L$  in ref. 38, in our disordered model ( $\xi \ll L$ ) the “near-field” region where the flux density is  $\alpha$ -dependent is limited only in the very close vicinity of the monopoles/antimonopoles.

Equations (47) and (48) are the Bohr quantization conditions, meaning that there are two localized states around  $x_2$  and  $x_3$  ( $\equiv x_1$ ), having the same energy. In general, when there are two localized states with the same energy, displaced each other by a high potential peak, there is a small tunnelling matrix element between them. It gives a small energy splitting between bonding and anti-bonding states. As a result, the degeneracy is lifted. Nevertheless, when the equality (46) holds, it guarantees that the hybridization between them cancels exactly, and the degeneracy is not lifted even after one takes the tunnelling into account. Thus the two localized states are in resonance with each other. Equation (49) means that such exact degeneracy occurs only when  $\alpha$  is equal to  $\pi$  or 0, confirming our numerical result.

If we change  $Q_1$  and  $Q_2$  to make  $S_1 \neq S_2$  with the conditions (47) and (48) preserved, there occurs a small splitting ( $\sim O(e^{-2S_i})$ ) to the otherwise degenerate states, due to a small unbalance between  $S_1$  and  $S_2$ . These conditions (47) and (48) specify one direction in the  $Q_1$ - $Q_2$  plane from the monopole. Along this direction the gap remains nonzero but very small, thereby the field  $\vec{F}$  becomes large as schematically shown in Fig. 15 (b). In our numerical results, this direction corresponds to the valley direction in the energy gap, and the ridge in the Thouless number in Fig. 14. Thus the anisotropy of the energy gap in the  $Q_1$ - $Q_2$  plane is of the order  $e^{2S_i} \sim e^{L/\xi}$ . Because in our numerical calculation  $L = 50$ ,  $\xi \sim 7$ , the anisotropy of the monopole is  $e^{2S_i} \sim e^{L/\xi} \sim e^7 \sim 10^3$ , which should be compared with the numerical value  $\sim 10$  in the previous subsection. Their difference can be attributed to finiteness of the mesh size in the numerical calculation; the mesh may not be fine enough to reproduce the anisotropy  $\sim 10^3$ . We also note that the strings observed in the numerical calculation can be regarded as the curve of  $\omega = (2n+1)\pi$ ,  $\omega' = (2n'+1)\pi$ , with  $S_1$  and  $S_2$  are unrestricted.



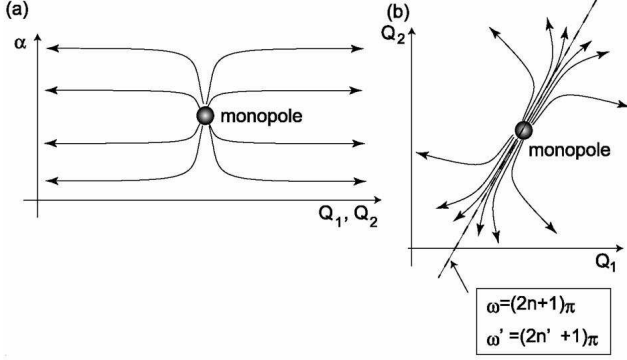


FIG. 15: Distribution of the vector field  $\vec{F}$  around the monopole. (a) the field  $\vec{F}$  is mostly uniform in the  $\alpha$ -direction because  $\xi \ll L$ , except for the vicinity of the monopole. (b) the field is anisotropic in the  $Q_1$ - $Q_2$  plane.

### Discussion

In Fig.(13f), we show the wave functions of the HOMO and LUMO, which supports the resonance tunnelling scheme. At the resonance, the energy of HOMO and LUMO are degenerate. If HOMO sits at  $x_1$ , LUMO can be viewed as the resonance state at the potential valley  $x_2$ . Therefore, by means of LUMO, HOMO can tunnel through the whole sample. We must emphasize that this mechanism is topological as that in the pure case.

The adiabatic rate depends on the energy gap. At the resonance, the wave functions of the HOMO and the LUMO do not overlap. By tuning the parameters, the overlapping integral between these two states are not zero, and thus the gap opens up. Again, the rates that the gap opens with the parameters are not necessarily the same. Therefore, the monopole (antimonopole) structure is not necessarily isotropic. In fact, it can be highly anisotropic as shown in our calculation. Then, the adiabatic rate is restricted by the minimal gap along the contour. It can be roughly estimated as  $e^{-L/\xi_R}$ , where  $\xi_R$  is the localization length at the resonance.

The current results for the periodic/twisted boundary condition is consistent with those for the open boundary condition. The topological structure in the open boundary condition, namely the vortices, can be regarded as a projection of the monopoles to a 2-dimensional plane. The anisotropic flux distribution and the anisotropic phase gradient are two facets of the resonance tunnelling. While the results for the open boundary condition is more applicable to the real materials and design, the non-trivial generation of the monopole-anti-monopole shown in the periodic/twisted boundary condition case illustrates the deep and whole new topological structure in

the strong disordered systems.

### CONCLUSION

In this paper, we have studied the charge pumping and dielectric response in disordered insulator for both the open boundary condition and periodic/twisted boundary condition. As for the open system coupled to the leads, we have found the quantum-mechanically enhanced dielectric response in nanoscopic/mesoscopic disordered insulators, which give a guide for fast and low-dissipation ferroelectric thin films of the FeRAM. The phase of the reflection coefficient  $r$  is a key parameter for the pumping, and has the rich structure in the parameter plane. Topological nature of the insulator dictates the phase winding of  $r$ , around the vortex where  $r = 0$  and  $|t| = 1$ . In a pure insulator, this corresponds to the gapless point. In the disordered case, it corresponds to the resonance tunnelling through the sample, whose position varies with the chemical potential.

With the periodic closed system, we can consider the three dimensional parameter space  $\vec{Q} = (Q_1, Q_2, \alpha)$  where  $Q_1$  is the site energy alternation,  $Q_2$  is the bond dimerization, and  $\alpha$  is the phase twist for the boundary condition. In this three dimensional space, one can discuss the monopoles and the their associated gauge field distribution, which are again interpreted in terms of the resonant tunnelling.

The existence of the resonant tunnelling in the parameter space is guaranteed by the topological properties of the charge pumping, and only two parameters such as  $Q_1$  and  $Q_2$  need to be tuned to realize it. These parameters can be controlled experimentally by the external electric field and pressure. Therefore the present theory offers a way to design the enhanced dielectric response in realistic systems by controlling the disorder.

The authors would like to thank D. Vanderbilt, S. Horiuchi, Y. Okimoto, Y. Ogimoto, and Y. Tokura for stimulating discussion. The work was partly supported by Grant-in-Aids under the Grant numbers 15104006, 16076205, and 17105002, and NAREGI Nanoscience Project from the Ministry of Education, Culture, Sports, Science, and Technology.

---

\* Electronic address: chern@issp.u-tokyo.ac.jp

- [1] R. Resta, Rev. Mod. Phys. **66**, 899 (1994).
- [2] R. M. Martin, Phys. Rev. B **9**, 1998 (1974).
- [3] R. Resta, Ferroelectrics **136**, 51 (1992).
- [4] R. D. King-Smith and D. Vanderbilt, Phys. Rev. B **47**, 1651 (1993).
- [5] G. Ortiz and R. M. Martin, Phys. Rev. B **49**, 14202 (1994).

- [6] S. Onoda, S. Murakami, and N. Nagaosa, Phys. Rev. Lett. **93**, 167602 (2004).
- [7] S. Murakami, S. Onoda, and N. Nagaosa (2007), unpublished.
- [8] D. J. Thouless, Phys. Rev. B **27**, 6083 (1983).
- [9] Q. Niu and D. J. Thouless, J. Phys. A **17**, 2453 (1984).
- [10] S. Onoda, C.-H. Chern, S. Murakami, Y. Ogimoto, and N. Nagaosa, Physical Review Letters **97**, 266807 (2006).
- [11] T. Egami, S. Ishihara, and M. Tashiki, Science **261**, 1307 (1993).
- [12] N. Nagaosa, J. Phys. Soc. Japan **55**, 2754 (1986).
- [13] P. Monceau, F. Y. Nad, and S. Brazovskii, Phys. Rev. Lett. **86**, 4080 (2001).
- [14] J. F. Scott, *Ferroelectric Memories* (Springer, 2000).
- [15] P. A. Lee and T. V. Ramakrishnan, Rev. Mod. Phys. **57**, 287 (1985).
- [16] L. E. Cross, Ferroelectrics **76**, 241 (1987).
- [17] Q. M. Zhang, V. Bharti, and X. Zhao, Science **280**, 2101 (1998).
- [18] S. Horiuchi, R. Kumai, Y. Okimoto, and Y. Tokura, Phys. Rev. Lett. **85**, 5210 (2000).
- [19] G. Gruner, Rev. Mod. Phys. **60**, 1129 (1988).
- [20] M. Switkes, C. M. Marcus, K. Campman, and A. G. Gosard, Science **283**, 1907 (1999).
- [21] Y. Levinson, O. Entin-Wohlman, and P. Wolfre, Physica A **302**, 335 (2001).
- [22] O. Entin-Wohlman and A. Aharony, Phys. Rev. B **66** (2002).
- [23] V. Kashcheyevs, A. Aharony, and O. Entin-Wohlman, Phys. Rev. B **69** (2004).
- [24] S. Datta, *Electronic Transport in Mesoscopic Systems* (Cambridge, 1995).
- [25] A. Aharony, O. Entin-Wohlman, and Y. Imry, J. Phys. Soc. Jpn. **72** (Suppl. A), 112 (2002).
- [26] P. W. Brouwer, Phys. Rev. B **58**, 10135 (1998).
- [27] M. Büttiker and A. Prêtre, Z. Phys. B **94**, 133 (1994).
- [28] J. E. Avron, A. Elgart, G. M. Graf, and L. Sadun, J. Stat. Phys. **116**, 425 (2004).
- [29] P. W. Anderson, Phys. Rev. **109**, 1492 (1958).
- [30] F. J. Wegner, Z. Phys. **25**, 327 (1976).
- [31] E. Abrahams, P. W. Anderson, D. C. Licciardello, and T. Ramakrishnan, Phys. Rev. Lett. **42**, 673 (1979).
- [32] A. MacKinnon and B. Kramer, Phys. Rev. Lett. **47**, 1546 (1981).
- [33] M. Y. Azbel, Phys. Rev. B **28**, 4106 (1983).
- [34] W.-K. Shih and Q. Niu, Phys. Rev. B **50**, 11902 (1994).
- [35] F. S. Galasso, in *International Series of Monographs in Solid State Physics* (Oxford, 1970), vol. 7.
- [36] S. Asanuma, M. Fukunaga, Y. Uesu, R. Haumont, B. Dkhil, C. Malibert, and J.-M. Kiat, Jpn. J. Appl. Phys. **43**, 6581 (2004).
- [37] A. Zee, Phys. Lett. B **135**(4), 307 (1984).
- [38] D. Cohen, Phys. Rev. B **68**, 155303 (2003).